

Wide Frequency Tuning of Continuous Terahertz Wave Generated by Difference Frequency Mixing under Exciton-Excitation Conditions in a GaAs/AlAs Multiple Quantum Well

Osamu Kojima,^{1,*} Yuki Tarui,¹ Hideaki Shimazu,¹ Takashi Kita,¹ Avan Majeed,² Pavlo Ivanov,^{2,3} Edmund Clarke,² and Richard Hogg^{2,3}

¹*Department of Electrical and Electronic Engineering, Kobe University, 1-1 Rokkodai, Nada, Kobe 657-8501, Japan*

²*Department of Electronic and Electrical Engineering, University of Sheffield, Sheffield S3 7HQ, United Kingdom*

³*Department of Electronic and Nanoscale Engineering, University of Glasgow, Glasgow G12 8LT, United Kingdom*

 (Received 2 May 2018; revised manuscript received 12 September 2018; published 12 October 2018)

Continuous terahertz wave sources with narrow bandwidth and wide frequency tunability enable high-resolution terahertz spectroscopy and high-speed information communication. In this study, using the optical nonlinearity of excitons as the source of second-order nonlinear polarization, we realize a continuous terahertz electromagnetic wave demonstrating wide frequency tunability from 0.1 to 18 THz without a decrease in intensity due to phonon scattering. Because of excitation of two exciton states in a GaAs/AlAs multiple quantum well using two continuous-wave lasers, terahertz waves are emitted as a result of difference-frequency mixing, where the intensity shows a square dependence on the excitation intensity. Using the inhomogeneous width of exciton lines, we achieve wide frequency tunability without phonon effects.

DOI: [10.1103/PhysRevApplied.10.044035](https://doi.org/10.1103/PhysRevApplied.10.044035)

I. INTRODUCTION

Excitons are good candidates for the source of various optical devices [1,2]. While the exciton in bulk group III–group V semiconductors is said to be unstable at room temperature because of the small binding energy, characteristics such as the transition energy and the oscillator strength can be controlled over a wide energy range. The optical nonlinearity of excitons is particularly important in device applications. When the second-order optical nonlinearity of GaAs crystals is focused, it is studied by observation of second-harmonic generation [3–7]. The second-order nonlinear optical polarization also causes difference-frequency mixing (DFM). The DFM process is a good wavelength-conversion method for generating terahertz electromagnetic waves [8–14], and therefore the enhancement of the second-order polarization is vital. For example, a perturbation such as an electric field is used to enhance the polarization by breaking the envelope-function symmetry [10,15], which generates longitudinal polarization. Furthermore, the electric field enhances the second-order nonlinear polarization via third-order optical nonlinearity, $P(\omega_1 \pm \omega_2) = \chi^{(3)}E(\omega_1)E(\omega_2)E(0)$ [16], where $\chi^{(3)}$ is the third-order nonlinear susceptibility, ω is

the frequency, and E is the electric field. Therefore, the electric field is important.

Although quantum-cascade lasers are the most-well-established continuous-wave terahertz sources [17,18], we focus on DFM using two external lasers. While it is difficult to change the frequency of quantum-cascade lasers considerably, the DFM frequency can be easily changed by the tuning of the energy separation of the two lasers. Moreover, a photomixer is a good converter of light to terahertz waves via the DFM process [8,13]; however, strong frequency dependence has been demonstrated. Considering the inhomogeneous width in quantum-confinement systems, the use of excitons in nanostructured semiconductors can be a good candidate for wide frequency tuning. By the breaking of the envelope-function symmetry caused by the applied field, the second-order nonlinear polarization of the excitons is enhanced, and the third-order nonlinear polarization will assist the enhancement. The advantage of using DFM is that while DFM using photoconductive antennas shows a large fall in intensity with increase in the frequency [8,9,13], the optical nonlinearity of excitons will maintain the intensity over a wide frequency range within the inhomogeneous width. Continuous-wave terahertz sources with a narrow spectral width and wide frequency tunability will be applied in high-resolution terahertz spectroscopy and information communication. In

*kojima@phoenix.kobe-u.ac.jp

this study, we demonstrate the wide tunability of a continuous terahertz wave generated by the DFM process under exciton-excitation conditions in a GaAs/AlAs multiple quantum well (MQW). When two lasers are described as $E_1 \exp[i(k_1x - \omega_1t)]$ and $E_2 \exp[i(k_2x - \omega_2t)]$, the terahertz wave generated by the DFM process is described as $E_1E_2 \exp[i(k_1 - k_2)x - i(\omega_1 - \omega_2)t]$ or $E_1E_2 \exp[i(k_2 - k_1)x - i(\omega_2 - \omega_1)t]$, where E_1 and E_2 are the amplitude of laser light, t is time, k_1 and k_2 are the wavevectors, and x is the position. On the basis of this relationship, the terahertz wave emitted along the direction of $k_1 - k_2$ ($k_2 - k_1$) is detected. When the two laser directions are the same, the direction of the terahertz wave is the same as the direction of the lasers. The excitation-energy dependence shows the resonant profile at the heavy-hole- (HH) exciton energy. At the light-hole- (LH) exciton energy, the increase in the excitation intensity leads to the appearance of the terahertz wave by the DFM process. The intensity also shows a square dependence on the excitation intensity in the exciton-excitation conditions. This square dependence originates from the second-order nonlinearity because the amplitude of the terahertz wave is given by E_1E_2 , as mentioned above. We examine the generation of the continuous terahertz wave in a wide frequency region from the perspective of exciton resonant effects in the inhomogeneous width.

II. EXPERIMENTS

We use an undoped GaAs/AlAs MQW embedded in a p - i - n structure on a (001) n^+ -doped GaAs substrate grown by molecular-beam epitaxy. The thickness of the surface p -doped GaAs layer with a doping concentration of $1 \times 10^{18} \text{ cm}^{-3}$ is 50 nm and that of the n -doped $\text{Al}_{0.4}\text{Ga}_{0.6}\text{As}$ layer with a doping concentration of $3 \times 10^{18} \text{ cm}^{-3}$ is 1500 nm. The MQW consists of 30 periods of GaAs and AlAs layers whose thickness is 7.35 nm. The 50-nm p -doped layer can reduce the absorption by the carrier and maintain the electric field [19]. The built-in field estimated from the doping concentrations is 20.6 kV/cm. The measurements of the terahertz wave are performed at 297 K. A semiconductor laser with a fixed photon energy of 1.506 eV and a continuous-wave mode Ti:sapphire laser (to change the excitation photon energy from 1.460 to 1.580 eV) are used; these are referred as L_1 and L_2 , respectively. The typical laser line widths of L_1 and L_2 are 0.21 and 0.14 meV, respectively. The experimental setup is shown in Fig. 1. The two beams are combined on a half mirror in free space with the same polarization, and the combined beam is focused on the sample surface through a hole in the off-axis parabolic mirror by a polymethylpentene lens, which is also used to collimate the emitted electromagnetic wave. A Si wafer is used to eliminate the contribution of the laser light to the signal. The excitation power is controlled by a variable neutral-density

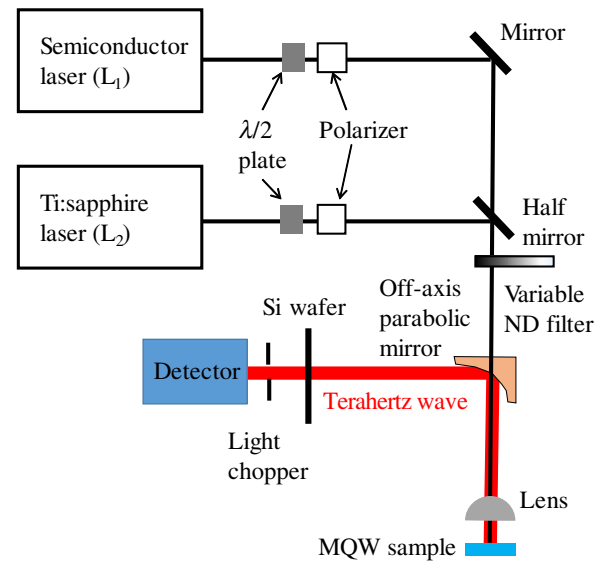


FIG. 1. The experimental set-up. Two laser beams are combined on a half mirror.

filter. The terahertz signal is detected by a pyroelectric sensor (THZ21-BL-BNC, Gentech-EO) and amplified by a lock-in-amplifier at 5 Hz. The exciton energies are evaluated from the conventional photoluminescence and photoreflectance spectra.

III. RESULTS AND DISCUSSION

Figure 2(a) shows the dependence of the signal intensity on the photon energy of L_2 . The photon energy of L_1 is constant at 1.506 eV, corresponding to the HH-exciton energy (as indicated by the vertical arrow). The broken vertical lines indicate the HH- and LH-exciton energies evaluated from the photoluminescence spectrum shown in Fig. 2(b). While the excitation intensity of L_1 is kept at 3.40 kW/cm^2 , the excitation intensity of L_2 is altered. An exciton density of approximately 10^{13} cm^{-3} for one laser is assumed in this excitation-intensity region. In all conditions, the resonant peak is observed at the HH-exciton energy. In general, in semiconductors with zinc-blende structure, the oscillator strength of the HH exciton is 3 times larger than that of the LH exciton. Therefore, when the signal intensity simply depends on the oscillator strength, the peak structure should be also observed at the LH-exciton energy. However, the peak structure is not clear at the LH-exciton energy. Furthermore, the intensity increases around 1.56 eV. In the photoreflectance spectrum, the signal due to the transition from the HH subband with a quantum number of 2 (HH2) to the electron subband is observed. Therefore, the increase in the intensity results from the resonant effect on this exciton state. As indicated by the horizontal arrows, the wider tunability of the terahertz wave is realized without the phonon dip at around 8.8

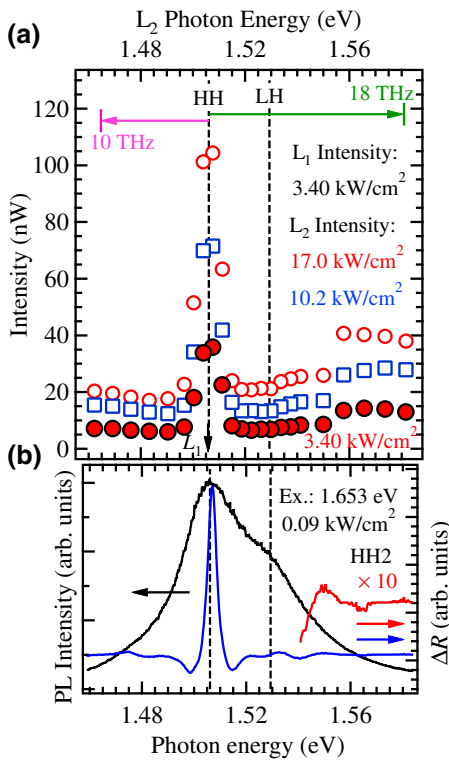


FIG. 2. (a) Signal intensity as a function of L₂ photon energy with various L₂ intensity settings. The L₁ photon energy is indicated by the vertical arrow and the power is kept at 3.40 kW/cm². As indicated by the closed circles, open squares, and open circles, the L₂ intensity is changed to 3.40, 10.2, and 17.0 kW/cm², respectively. The broken lines indicate the exciton energies of the HH and LH excitons. (b) The photoluminescence (PL) and photoreflectance spectra.

THz, which is the frequency of a longitudinal optical (LO) phonon in GaAs.

When the signals originate from the terahertz wave generated by the DFM process, the intensity depends on the square of the excitation intensity, where the maximum excitation intensity is limited by the L₁ output. The excitation-intensity dependence is measured as shown in Fig. 3(a). While the lasers are tuned to the HH- and LH-exciton energies, the intensity ratio is changed from 1:1 to 1:5. The broken lines indicate the gradient of the square dependence, and the vertical gray line represents the measurement conditions in Fig. 2(a); for example, the result at 17.0 kW/cm² in Fig. 2(a) corresponds to a ratio of 1:5 (indicated by the red circles on the vertical line). The signal intensity in all conditions shows the square dependence of the excitation-intensity after showing a linear dependence. This result demonstrates that the signal with a square dependence originates from the terahertz wave caused by the DFM process due to the second-order optical nonlinear polarization. Thermal radiation due to exciton and/or carrier-phonon interaction contributes significantly to the

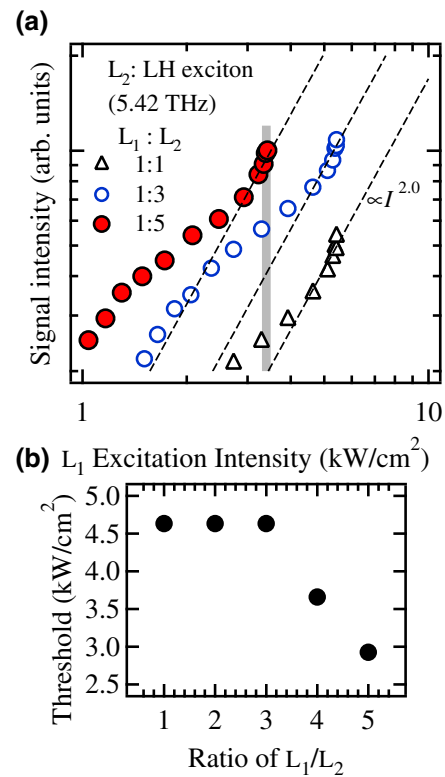


FIG. 3. (a) Excitation-intensity dependence of the signal intensity. The broken lines indicate the gradient of the square dependence. The open triangles, open blue circles, and closed red circles indicate the intensity measured at ratios of 1:1, 1:3, and 1:5, respectively. (b) The threshold value as a function of the laser-intensity ratio.

signals observed in the linear-increase region; for example, the signals of 3.40 and 10.2 kW/cm² at the LH-exciton energy.

The shift of the threshold value appearing as the square dependence of the lower L₂ powers in Fig. 3(a) suggests the effects of the oscillator-strength ratio of the LH and HH excitons. The threshold value is plotted as a function of the ratio of laser powers in Fig. 3(b). When the L₂ intensity is more than 3 times greater than that of L₁, the threshold intensity of L₁ decreases. Considering that the oscillator strength of the HH exciton is 3 times greater than that of the LH exciton, this decrease results from the ratio of the exciton-oscillator strengths between the HH and LH excitons. The intersubband transition is also the origin of the shift. Namely, in addition to the difference in the oscillator strengths, because of the intersubband transition, the lifetime and/or dephasing time of the LH exciton is shorter than for the HH exciton, so a larger excitation power of L₂ is required. Furthermore, the signal intensity at the HH2-exciton energy is larger than that at the LH-exciton energy. Considering that the oscillator strength of the HH2-exciton is smaller than that of the LH exciton, there is a possibility

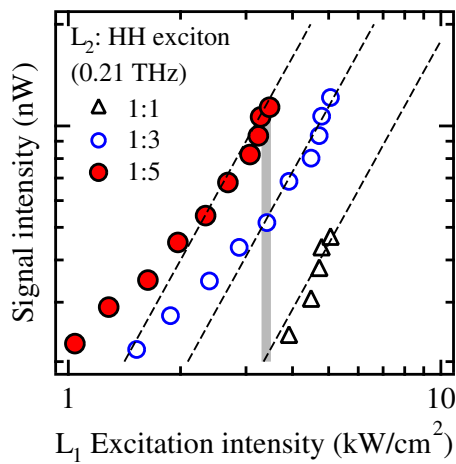


FIG. 4. Excitation-intensity dependence of the signal intensity. The broken lines indicate the gradient of the square dependence. The open triangles, open blue circles, and closed red circles indicate the intensity measured with ratios of 1:1, 1:3, and 1:5, respectively.

that the difference in the Bloch-function forms between the heavy and light holes is related to the intensity.

Under the HH-exciton-excitation condition, the effect of the second-order nonlinear polarization is stronger. The excitation-density dependence is shown in Fig. 4, and the vertical gray line represents the measurement conditions in Fig. 2(a). When both intensities are the same, the intensity increases with the square of the power. This square dependence is not observed under the orthogonal polarization condition, as shown in Fig. 5, which is measured with an excitation-intensity ratio of 1:1. This result indicates that the signal at the HH-exciton energy in Fig. 2(a) originates from the terahertz wave. Here, considering that the thermal emission does not depend on the laser polarization, the intensities in both conditions are the same.

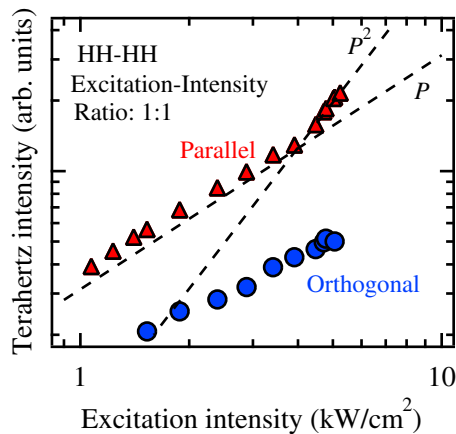


FIG. 5. Excitation-intensity dependence of the signal intensity measured under the different polarization conditions. The excitation-intensity ratio of the two lasers is 1:1.

However, even in the low-excitation-intensity region, the terahertz wave weakly contributes to the signal, and the thermal effect is superior to the effect of the terahertz wave. Therefore, the signal shows a linear dependence and is larger than that measured under the cross-polarization condition. These results demonstrate that the exciton number is closely related to the terahertz intensity.

The frequency of the terahertz wave can be measured with a Fabry-Perot interferometer that consists of two silicon wafers. By changing the distance between the wafers, we measure the interference signals, as shown in Figs. 6(a) and 6(b). The laser spectra are shown in the insets. To estimate the frequency, the spectra are fitted with a Gaussian function. The laser-intensity ratio in both measurements is 1:3. The terahertz signal is fitted with a sine function. The

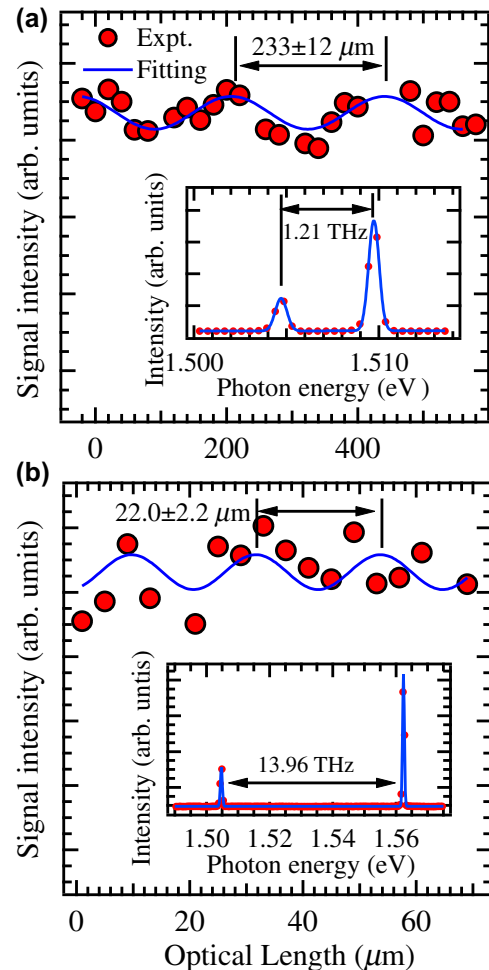


FIG. 6. The interference signal measured by the Fabry-Perot interferometer are indicated by the closed circles. The solid curves indicate the fitting results by the sine function. The insets are the laser spectra indicated by the closed circles and the results of the Gaussian fitting indicated by the solid curves. Both signals are measured with an excitation-intensity ratio of 1:3.

value of the horizontal axis is twice the wafer separation. The evaluated frequencies are 1.29 and 13.63 THz in the cases in Figs. 6(a) and 6(b), respectively. These almost agree with the frequencies estimated from the laser spectra. Therefore, the signals originate from the terahertz wave by the DFM process. However, the interference pattern is not strong. As the reasons, the small reflectivity of the silicon and thermal radiation are considered. The suppression of this thermal radiation should be solved for the application.

In Fig. 2(a), there is no intensity dip due to the LO phonon whose energy is approximately 37 meV, which is one advantage of using excitons to realize wide frequency tuning. When the second-order nonlinear polarization is generated by the electron-hole pair with use of photoconductive antennas, the intensity decreases beyond the LO-phonon frequency. The terahertz wave in the LO-phonon-frequency range cannot be emitted because of the absorption and *Reststrahlen* band [20]. However, as demonstrated by the horizontal arrows in Fig. 2(a), the use of excitons enables wide frequency tuning up to 18 THz. Since the terahertz emission obtained with photoconductive antennas is based on the drift current due to an external bias in most cases, scattering carriers by phonons decreases the intensity. On the other hand, with use of excitons in quantum well (QW) systems, the excitons related to the terahertz-wave emission are in different QWs, and the exciton interference generates the terahertz wave. This point (i.e., the interference occurs between the different QWs) may reduce the effect by the *Reststrahlen* band, which will need further study. Namely, wide frequency tuning is realized by use of exciton interference. In quantum-confinement systems, the fluctuation of the well width is unavoidable, which leads to the inhomogeneous width. Therefore, the HH exciton of a QW of nominal thickness and the LH or HH excitons in QWs of different thicknesses are excited under the excitation conditions of the energy separation corresponding to the LO-phonon energy. The interference of those excitons generates the terahertz wave. This is the reason why the intensity dip is not observed in our experiment.

In addition, although there are several absorption lines of water vapor [21,22], the absorption hardly affects the intensity profile in Fig. 2(a), where the measurement is made in a room with ambient humidity of less than 50%. As the reasons, the energy separation is not fine, and the line width of the terahertz wave may be broader than that of the water lines.

In terms of efficiency, with powers of L_1 of 3.40 kW/cm² and L_2 of 3.4, 10.0, and 17.0 kW/cm² in Fig. 2(a), a terahertz-wave intensity of approximately 36, 72, and 104 nW is achieved. Hence, an efficiency of 607, 404, and 350 $\mu\text{W}/\text{W}^2$ is estimated, which suggests that the thermal effect reduces the efficiency. Considering that only the asymmetric envelope function caused by the

quantum-confined Stark effect due to the built-in field is used, the efficiency can be regarded as high.

IV. CONCLUSION

We investigate the generation of a continuous terahertz wave with wide frequency tunability in the exciton-energy region of a GaAs/AlAs MQW. When the lasers excite the excitons, the terahertz wave is generated by the DFM process. The laser-energy dependence shows a frequency tuning range of 18 THz without an intensity decrease caused by the LO phonon. Furthermore, in addition to the exciton-oscillator strength, the exciton dephasing is closely related to the terahertz intensity. We can expect further intense terahertz generation due to the optimization of the structure. Therefore, considering that the line width of the terahertz wave is determined by the line widths of the excitation lasers, a wide-frequency tunable terahertz wave source with a narrow line width will be realized with the DFM process based on excitons, for instance, which can be applied for high-resolution terahertz spectroscopy.

ACKNOWLEDGMENTS

We acknowledge financial support provided by the Japan Society for the Promotion of Science KAKENHI program (Grants No. JP26289088 and No. 16KK0129).

-
- [1] D. S. Chemla, D. A. B. Miller, P. W. Smith, A. C. Gossard, and W. Wiegmann, Room temperature excitonic nonlinear absorption and refraction in GaAs/AlGaAs multiple quantum well structures, *IEEE J. Quantum Electron.* **20**, 265 (1984).
 - [2] A. M. Fox, A. C. Maciel, J. F. Ryan, and T. Kerr, Nonlinear excitonic optical absorption in GaSb, *Appl. Phys. Lett.* **71**, 193 (1997).
 - [3] R. K. Chang, J. Ducuing, and N. Bloembergen, Dispersion of the Optical Nonlinearity in Semiconductors, *Phys. Rev. Lett.* **15**, 415 (1965).
 - [4] H. Lotem, G. Koren, and Y. Yacoby, Dispersion of nonlinear optical susceptibility in GaAs and GaSb, *Phys. Rev. B* **9**, 3532 (1974).
 - [5] S. Bergfeld and W. Daum, Second-harmonic Generation in GaAs: Experiment versus Theoretical Predictions of $\chi_{xyz}^{(2)}$, *Phys. Rev. Lett.* **90**, 036801 (2003).
 - [6] F. Nastos and J. E. Sipe, Optical rectification and shift currents in GaAs and GaP response: Below and above the band gap, *Phys. Rev. B* **74**, 035201 (2006).
 - [7] D. Brunne, M. Lafrentz, V. V. Pavlov, R. V. Pisarev, A. V. Rodina, D. R. Yakovlev, and M. Bayer, Electric field effect on optical harmonic generation at the exciton resonances in GaAs, *Phys. Rev. B* **92**, 085202 (2015).
 - [8] K. A. McIntosh, E. R. Brown, K. B. Nichols, O. B. McMahon, W. F. DiNatale, and T. M. Lyszczarz, Terahertz photomixing with diode lasers in low temperature grown GaAs, *Appl. Phys. Lett.* **67**, 3844 (1995).

- [9] P. Gu, M. Tani, M. Hyodo, K. Sakai, and T. Hidaka, Generation of cw-terahertz radiation using a two-longitudinal-mode laser diode, *Jpn. J. Appl. Phys.* **37**, L976 (1998).
- [10] B. Rosam, K. Leo, L. Yang, and M. M. Dignam, Terahertz generation by difference-frequency mixing of exciton Wannier-Stark ladder states in biased semiconductor superlattices, *Appl. Phys. Lett.* **85**, 4612 (2004).
- [11] K. Morita, S. Katoh, T. Takimoto, F. Tanaka, Y. Nakagawa, S. Saito, T. Kitada, and T. Isu, Generation of terahertz radiation from two cavity modes of a GaAs/AlAs coupled multilayer cavity, *Appl. Phys. Express* **4**, 102102 (2011).
- [12] S. Preu, G. H. Döhler, S. Malzer, L. J. Wang, and A. C. Gossard, Tunable, continuous-wave terahertz photomixer sources and applications, *J. Appl. Phys.* **109**, 061301 (2011).
- [13] H. Tanoto, J. H. Teng, Q. Y. Wu, M. Sun, Z. N. Chen, S. A. Maier, B. Wang, C. C. Chum, G. Y. Si, A. J. Danner, and S. J. Chua, Nano-antenna in a photoconductive photomixer for highly efficient continuous wave terahertz emission, *Sci. Rep.* **3**, 2824 (2013).
- [14] T. Kitada, S. Katoh, T. Takimoto, Y. Nakagawa, K. Morita, and T. Isu, Terahertz emission from a GaAs/AlAs coupled multilayer cavity with nonlinear optical susceptibility inversion, *Appl. Phys. Lett.* **102**, 251118 (2013).
- [15] P. C. M. Planken, M. C. Nuss, I. Brener, K. W. Goossen, M. S. C. Luo, S. L. Chuang, and L. Pfeiffer, Terahertz Emission in Single Quantum Wells after Coherent Optical Excitation of Light Hole and Heavy Hole Excitons, *Phys. Rev. Lett.* **69**, 3800 (1992).
- [16] P. Godefroy, W. de Jong, C. W. van Hasselt, M. A. C. Devillers, and Th. Rasing, Electric field induced second harmonic generation spectroscopy on a metal-oxide-silicon structure, *Appl. Phys. Lett.* **68**, 1981 (1998).
- [17] T.-T. Lin, L. Ying, and H. Hirayama, Threshold current density reduction by utilizing high-Al-composition barriers in 3.7 THz GaAs/Al_xGa_{1-x}As Quantum cascade lasers, *Appl. Phys. Express* **5**, 012101 (2012).
- [18] F. Valmorra, G. Scalari, K. Ohtani, M. Beck, and J. Faist, InGaAs/AlInGaAs THz quantum cascade lasers operating up to 195 K in strong magnetic field, *New J. Phys.* **17**, 023050 (2015).
- [19] M. Nakayama, S. Asai, H. Takeuchi, O. Ichikawa, and M. Hata, Voltage-controllable terahertz radiation from coherent longitudinal optical phonons in a *p-i-n* diode structure of GaAs, *Appl. Phys. Lett.* **103**, 141109 (2013).
- [20] S. Kono, M. Tani, P. Gu, and K. Sakai, Detection of up to 20 THz with a low-temperature-grown GaAs photoconductive antenna gated with 15 fs light pulses, *Appl. Phys. Lett.* **77**, 4104 (2000).
- [21] Y. Yang, A. Shutler, and D. Grischkowsky, Measurement of the transmission of the atmosphere from 0.2 to 2 THz, *Opt. Express* **19**, 8830 (2011).
- [22] Y. Yang, M. Mandehgar, and D. Grischkowsky, Determination of the water vapor continuum absorption by THz-TDS and molecular response theory, *Opt. Express* **22**, 4388 (2014).